



The effective Ni(II) removal of red mud modified chitosan from aqueous solution

Thi-Thuy Luu · Duy-Khoi Nguyen ·
Tu Thi Phuong Nguyen · Thien-Hoang Ho ·
Van-Phuc Dinh · Hoang Anh Tuan Kiet

Received: 19 November 2021 / Accepted: 17 December 2022 / Published online: 2 January 2023
© The Author(s), under exclusive licence to Springer Nature Switzerland AG 2023

Abstract This study used red mud modified with chitosan (RM/CS) as a novel adsorbent to remove Ni(II) ions from an aqueous solution. The adsorbent was characterized by the techniques of the BET method, X-ray diffraction (XRD), and scanning electron microscopy (SEM) analysis. According to the findings, the surface area of RM/CS is nearly doubled compared to CS, from 68.6 to 105.7 m².g⁻¹. The Ni(II) batch adsorption of RM/CS was performed as a function of pH value, contact time, and volume of adsorbent. Three isotherm adsorption models (Langmuir, Freundlich, and Sips) and three kinetic models (the pseudo-first-order, the pseudo-second-order, and the intra-diffusion models) were fitted with the experimental data to calculate the maximum adsorption capacity and to estimate the uptake in nature. The Langmuir

monolayer adsorption capacity for Nickel (II) is 31.66 mg.g⁻¹ at a pH of 6.0, with an adsorption time of 180 min and a temperature of 323 K. The Ni(II) adsorption on RM/CS is the exothermic process and is controlled by the intra-diffusion model.

Keywords Adsorption · Mechanism · Intra-diffusion model · Low-cost adsorbent

Introduction

In recent years, numerous studies have employed wastes from agricultural and industrial operations as adsorbents to limit environmental pollution concerns while also bringing economic advantages to society. Some adsorbents can be used in this process, such as shells, chitosan (Hamza et al., 2019; Pap et al., 2020; Vakili et al., 2019), lignin (Supanchaiyamat et al., 2019), and fly ash (Aigbe

Supplementary Information The online version contains supplementary material available at <https://doi.org/10.1007/s10661-022-10877-0>.

T.-T. Luu · D.-K. Nguyen · V.-P. Dinh (✉)
Future Materials & Devices Laboratory, Institute of Fundamental and Applied Sciences, Duy Tan University, Ho Chi Minh City 700000, Vietnam
e-mail: dinhvanphuc@duytan.edu.vn

T.-T. Luu · D.-K. Nguyen · V.-P. Dinh
Faculty of Natural Sciences, Duy Tan University, Da Nang 550000, Vietnam

T. T. P. Nguyen
Department of Chemistry, Faculty of Science, Chulalongkorn University, Payathai Road, Patumwan, Bangkok 10300, Thailand

T.-H. Ho
Dong Nai University, 4 Le Quy Don Street, Tan Hiep Ward, Dong Nai Province, Vietnam

H. A. T. Kiet (✉)
Department of Physics and Engineering, West Chester University of Pennsylvania, West Chester, PA 19383, USA
e-mail: ahoang@wcupa.edu

H. A. T. Kiet
Graduate School of Education, University of Pennsylvania, Philadelphia, PA 19104, USA

et al., 2021; Deng et al., 2018). One of the solid wastes in this category of materials is red mud, which is produced during the Bayer process of producing alumina from bauxite ore. Because sodium hydroxide solution is used to decompose the bauxite ore in the alumina manufacturing process (Khairul et al., 2019), the red mud has a pH range of 10 to 13. The composition of red mud mainly contains Fe_2O_3 , Al_2O_3 , Na_2O , SiO_2 , Na_2O , CaO , TiO_2 , and several rare elements (Khairul et al., 2019). These chemical compositions and alkalinity are the primary sources of environmental damage; 1 to 1.5 tons of red mud are discharged into the environment to create 1 ton of aluminum oxide (Khairul et al., 2019). Annually, the amount of red mud discharged is estimated at nearly 150 million tons (Khairul et al., 2019), resulting in the proper disposal of red mud as a significant challenge for the alumina industries. To deal with red mud thoroughly, red mud has been utilized as an adsorbent to remove pollutants such as heavy metal ions, dyes, and various inorganic anions (Taneez & Hurel 2019; Wang et al., 2019; Wang & Liu 2021). However, their adsorption capacity is not high because the characteristics of red mud significantly depend on their origin or where they are found (Khairul et al., 2019). Various methods have been conducted to modify red mud, such as acid treatment (Sahu et al., 2013; Smičiklas et al., 2014), heat treatment (de Jesus et al., 2015; Yang et al., 2020), and modification by synthetic polymers (Ni et al., 2015). Nonetheless, there have not been a number of studies on altering red mud materials with natural polymers that are both ecologically benign and low cost.

Nowadays, the development of various industries has produced a tremendous amount of waste containing hazardous and carcinogenic heavy metal ions, including Ni(II) ions. When Ni(II) concentrations in an aqueous solution surpass $0.07 \text{ mg}\cdot\text{L}^{-1}$, according to WHO, these ions become hazardous (Çelebi et al., 2020). Scientists have been working to discover effective and reasonably affordable ways to remove heavy metal ions from aqueous solutions due to the rising water pollution problem. Precipitation, reverse osmosis, extraction, and adsorption are some of the approaches that have been used (Bartczak et al., 2018). Because of the reusability of adsorbents via the desorption process, adsorption is one of the most effective ways of removing metal ions from an aqueous solution among the approaches mentioned above (Bartczak et al., 2018).

For the reasons stated above, the main objective of this study is to use red mud to enhance the surface area

of the chitosan and use the red mud/chitosan composite for the removal of Ni(II) from aqueous solutions. The physicochemical properties of materials were analyzed using modern analytical techniques. The factors affecting the Ni(II) removal of this material were also examined, consisting of pH solution, contact time, and adsorbent dosage. In particular, the uptake of Ni(II) ions by RM/CS in nature was also investigated in detail based on the combination of adsorption isotherm, kinetic models, and thermodynamic studies. Furthermore, since the red mud's disposal generates environmental pollution, its reuse and development to become an excellent adsorbent, which is low-cost and environmentally friendly, will positively affect the surrounding environment.

Experimental

Materials and chemicals

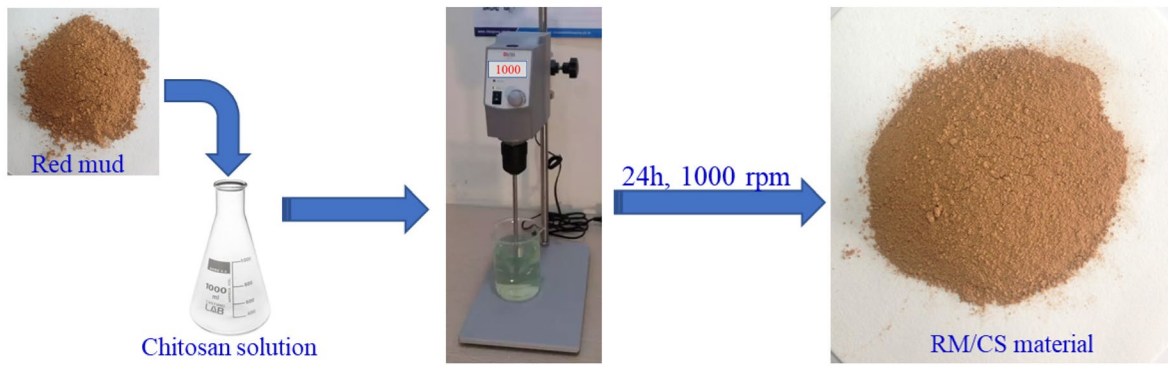
Chitosan (flake form, yellow color) was synthesized by a research team from the Institute of Nuclear Research, Da Lat, Vietnam, with the following parameters: moisture content of 12.5%, acetylation degree of 90%, and molecular weight of 91.7 kDa. Red mud (RM) used in these experiments is taken from the waste of the Saigon underground water plant in Ho Chi Minh City, Vietnam. Other chemicals used in these experiments were purchased from Merck, including nickel standard solution $1000 \text{ mg}\cdot\text{L}^{-1}$, acid nitric HNO_3 63%, sodium hydroxide NaOH 98%, and DI water.

Preparation of RM/CS

Red mud/chitosan material (RM/CS) was prepared according to the procedure shown in Scheme 1. Herein, 10.0 g of red mud was placed in 100 mL of chitosan solution containing 2.0 g of chitosan dissolved in 2% acetic acid solution. Next, the obtained mixture was stirred at 1000 rpm for 24 h to complete the modification. Thereafter, the resulting RM/CS mixture was centrifuged at 5000 rpm and washed with DI water several times before drying at 100°C for 24 h.

Instruments

The structures of RM before and after modification with chitosan were determined using powder X-ray diffraction (D2-Phaser, Bruker, USA) equipped with a $\text{Cu-K}\alpha$



Scheme 1 The procedure of preparing RM/CS material

radiation source of $\lambda=1.5406 \text{ \AA}$. The surface areas of RM and RM/CS materials were measured by the BET surface area analyzers (Quantachrome NOVA 1000e, USA), whereas the morphologies of these materials were observed using a scanning electron microscope (SEM) (S-4800, Hitachi, Japan).

pHpzc of the adsorbent was examined according to the salt addition method (Lyklema, 1984). To begin with, 0.1 g RM/CS was placed into each beaker, including 50.0 mL of 0.1 M NaCl. The pH values were adjusted using a pH meter (SI Analytics Lab 875, Germany) between 2 and 12 (± 0.1 pH units) with 0.1 M HNO_3 or 0.1 M NaOH. Next, these solutions were stirred for 24 h until the equilibrium was obtained, and then measure the pH again. The line graph of the initial pH (pHo) versus the difference between the initial and final pH values (ΔpH) and the pHpzc was determined at the point where $\text{pH}=0$.

Batch adsorption investigation

The standard nickel solution (1000 mg.L^{-1}) was used to make Ni(II) solutions with defined concentrations. The pH values of this solution were adjusted using 1 M HNO_3 and 1 M NaOH. Next, 0.1 g ($\pm 0.0001 \text{ g}$) of RM/CS adsorbent was added to a series of beakers containing 50 mL of the prepared Ni(II) solution. Then, the adsorption process was performed at constant speed on a 10-point magnetic stirrer (RSM-03-10 K, Phoenix Instrument, Germany). Effects of pH (2–6), contact time (5–240 min), and mass of adsorbent (0.05–0.25 g) were carried out to find out the optimal conditions. The concentration ranges ($20\text{--}120 \text{ mg.L}^{-1}$) and temperatures (298 K, 313 K, 323 K) were used during the

isotherm and thermodynamic study. After stirring, the solution was filtered and diluted with the appropriate dilution factor. The concentrations of Ni(II) before and after adsorption were analyzed by the AAS method (AAS-6300, Shimadzu, Japan). The adsorption capacity (Q_e) and elimination efficiency ($\%H$) of Ni(II) ions were determined according to the following formulas:

$$Q_e = \frac{(C_o - C_e) \times V}{m}, \tag{1}$$

$$\%H = \frac{(C_o - C_e) \times 100\%}{C_o}, \tag{2}$$

where C_o (mg.L^{-1}) and C_e (mg.L^{-1}) are initial and final concentrations of Ni(II) before and after the adsorption process; V (L) and m (g) are the volume of Ni(II) solution and the dosage of RM/CS, respectively.

Results and discussion

Physicochemical characteristics of RM/CS

The BET surface area of RM and RM/CS are shown in Fig. 1a, b, respectively. Results inform that the modification significantly enhances the surface area of RM with chitosan. RM, in particular, has a surface area of $68.6 \text{ m}^2 \cdot \text{g}^{-1}$. The surface area of the modified material reaches $105.7 \text{ m}^2 \cdot \text{g}^{-1}$ after chitosan modification. Clearly, chitosan molecules act as frames to support the structure of the red mud, resulting in increasing the porosity of the material. Consequently, this finding shows that chitosan helps increase the surface area of RM, therefore

increasing its adsorption effectiveness (Luu et al., 2022). Furthermore, the adsorption–desorption curves in these figures indicate that both materials are mesoporous and suitable for adsorption (Zhu et al., 2017).

Figure 1c, d shows SEM images of RM and synthesized RM/CS, respectively. RM has a flat and smooth surface, and the particles bind together to form a block, as seen in this diagram. On the contrary, RM/CS shows a porous and rough surface. These results are also consistent with BET analysis, which suggests that the synthesized RM/CS material is convenient and beneficial for the adsorption of heavy metals.

X-ray diffraction (XRD) patterns of RM and RM/CS are shown in Fig. 2. It can be seen from curve (a) that RM includes several phases, such as calcite (CaCO_3), quartz (SiO_2), sodalite ($\text{Na}_2\text{O} \cdot \text{Al}_2\text{O}_3 \cdot \text{SiO}_2$), and andradite (hydrated) ($\text{Ca}_3(\text{Fe}_{0.87}\text{Al}_{0.13})_2(\text{SiO}_4)_{1.65}(\text{OH})_{5.4}$) (Li et al., 2019). After the modification of chitosan, there are changes in the intensities of characteristic peaks in

the XRD pattern of RM without the appearance of new peaks. It confirms that RM has been successfully modified by CS, which plays as a supporting frame increasing the RM's surface area.

From the results above, a novel material was formed based on the modification of RM by CS. This leads to changes in the properties of RM as well as CS, especially surface characteristics. Herein, red mud acted simultaneously as an alkalinity regulator and reacted with chitosan to form the novel material, leading to the creation of many active adsorption sites. This results in enhancing the adsorption capacity.

Effects of some factors on the Ni(II) adsorption

Effect of pH

The point of zero charge (pH_{PZC}) is a significant value to depict the dependence of the pH values on the charge

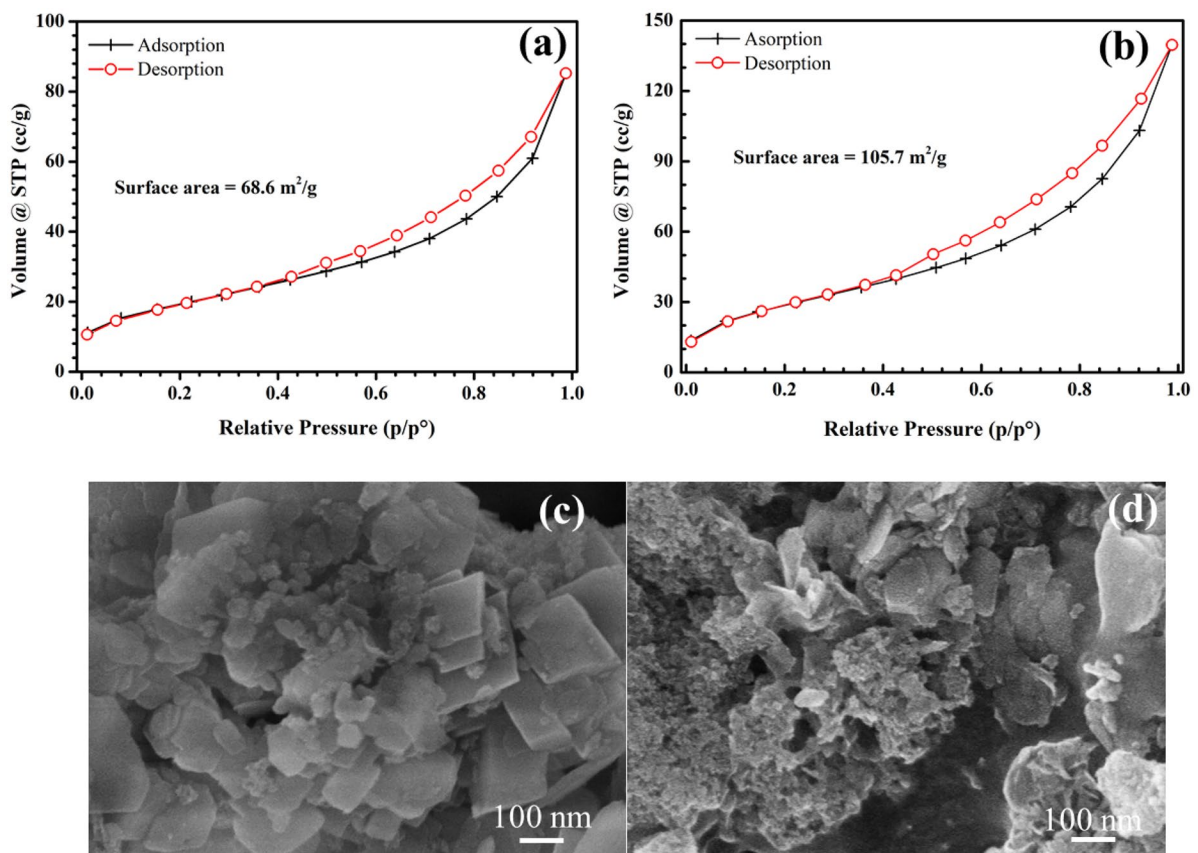


Fig. 1 BET surface area of RM (a) and RM/CS (b); SEM images of RM (c) and RM/CS (d)

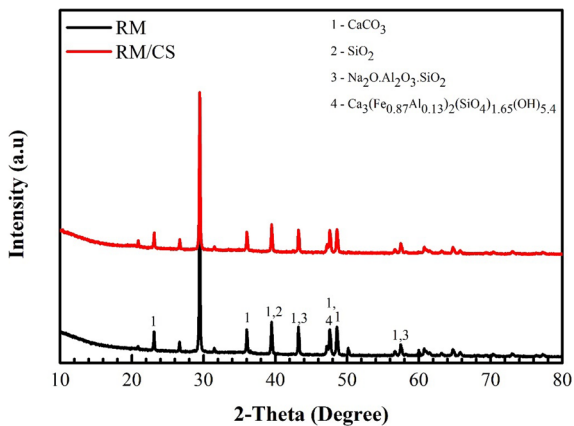


Fig. 2 XRD curves of RM and RM/CS

on the surface of the material. At pH values less than pH_{PZC} , the material’s surface will be positively charged, and vice versa for pH values above the pH_{PZC} (Zhang et al., 2016). As observed in Fig. 3a, pH_{PZC} is found at a pH of 6.1. The research work of Fei Lyu et al. reported that the pH_{PZC} for red mud modified by colloidal silica and sodium hydroxide was 7.59 (Lyu et al., 2021). In contrast, Tianxue Yang et al. reported the pH_{PZC} of red mud and heat-modified red mud at 900 °C to be 9.8 and 9.5, respectively (Yang et al., 2020).

Since it is an essential factor affecting the removal of heavy metal ions, the effect of pH solution on the Ni(II) removal of RM/CS material was examined at different initial pH levels varying from 2 to 6. From Fig. 3b, RM/CS witness a dramatic increase in the adsorption capacity from pH=2 to pH=6. This behavior of a material can be explained using pH_{PZC} . Because of interactions between functional groups and protons at low pH, the material’s surface exhibits positive charges in the pH range of our study (Khajavian et al., 2019). As a result, Ni(II) ions compete with protons on the material surface at low pH levels during the adsorption process, resulting in a considerable loss in adsorption efficiency.

On the other hand, there is strong repulsive interaction among the cations in this case due to a large number of positively charged sites on the material’s surface. As a result, the Ni(II) adsorption on the material’s surface has interfered, and a low adsorption capacity is achieved. The number of negatively charged sites rises by further increasing pH value, thus increasing the electrostatic interactions between Ni(II) ions and negatively charged sites of the material’s surface. This leads to the

improvement of removal efficiency (Khajavian et al., 2019). In this study, the Ni(II) adsorption efficiency reached the highest value at pH=6, so it was chosen as the optimal pH for the Ni(II) adsorption of RM/CS.

Effect of contact time

The effect of adsorption time was investigated by varying the contact time between 5 and 240 min. As shown in Fig. 3c, the Ni(II) removal efficiency increases as a function of time and reaches maximum efficiency at around 180 min. However, the adsorption rate is quick at the beginning, and it slows down after 20 min, which may be ascribed to the fact that there are plenty of adsorption sites on the material’s surface in the early stages. Then these adsorption sites gradually decrease during the adsorption process, resulting in a decreasing uptake rate. It is noteworthy that the Ni(II) adsorption obtained the equilibrium after 180 min. Thus, 180 min was chosen as the optimal adsorption time.

Effect of dosage of adsorbent

Figure 3d presents the effect of RM/CS material on the Ni(II) adsorption capacity. As the weight of the material rises from 0.05 to 0.25 g, the adsorption efficiency gradually rises from 36.21 to 81.33%. This result can be interpreted by a large number of adsorption sites that are present in the system. Accordingly, the increasing adsorbent amount would lead to the enhancement of adsorption sites, whereas the Ni(II) adsorbate concentration remains constant. Consequently, the uptake capacity and the removal efficiency of Ni(II) are enhanced.

Adsorption kinetics

In order to investigate the Ni(II) adsorption kinetics of RM/CS, the experimental data were fitted with three kinetic models, including pseudo-first-order, pseudo-second-order, and intra-diffusion kinetic models. Figure 4a describes the Ni(II) adsorption capacity of RM/CS after varying contact times, and the curves are suitable for three of these kinetic models. At the same time, Supplementary Table S1 presents the calculated kinematic parameters using a nonlinear method. The results reveal the high agreement of the intra-diffusion kinetic model with the experimental data via the correlation coefficient R^2 , RMSE, and χ^2 error function values are 0.9582, 0.3877, and 0.1752, respectively. Owing to the excellent

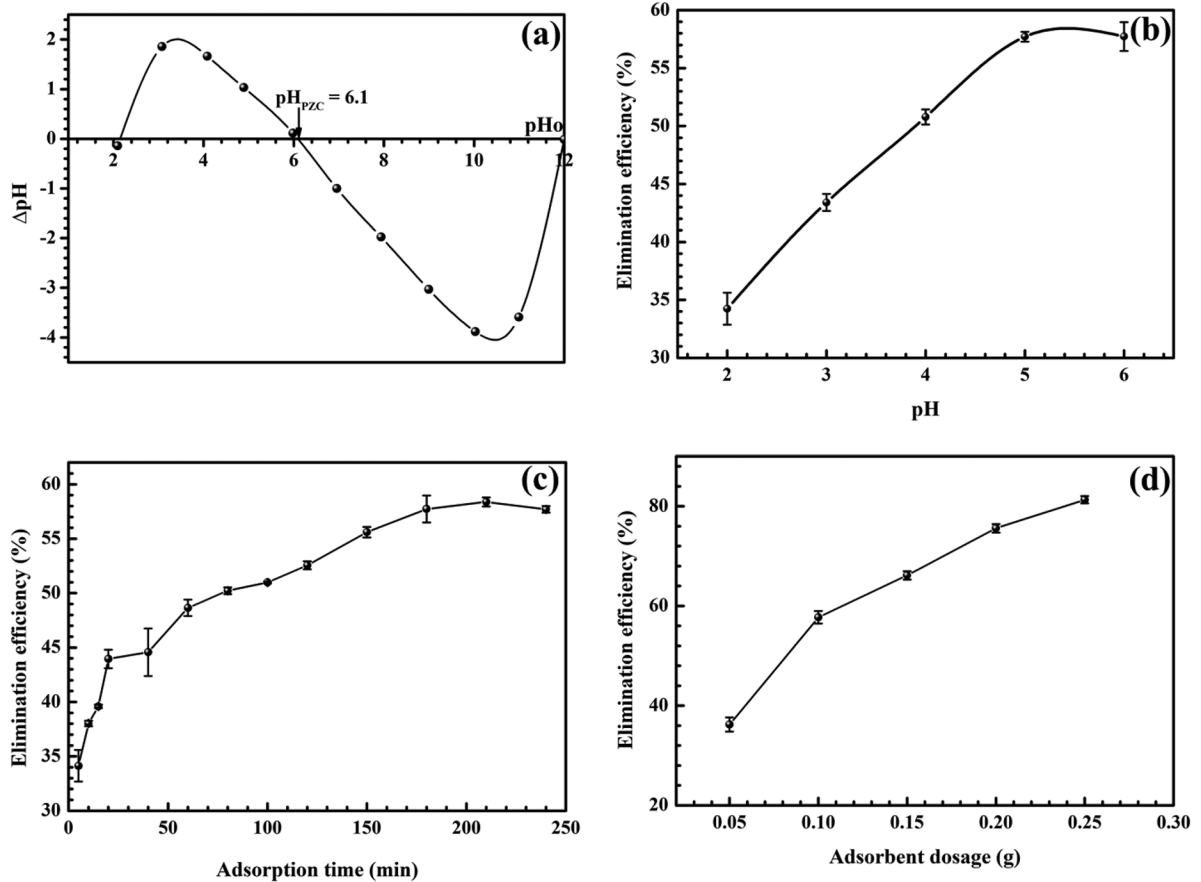
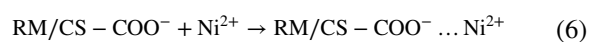


Fig. 3 pH_{PZC} of RM/CS (a); effects of pH (b), adsorption time (c), and adsorbent dosage (d) on the Ni(II) uptake of RM/CS (initial concentration = $50 \text{ mg}\cdot\text{L}^{-1}$, adsorbent mass = 0.1 g , shaking speed = 150 rpm)

fit of the intra-diffusion kinetic model to the experimental data and the non-zero value of C , it is expected that the Ni(II) adsorption of RM/CS occurs via different mechanisms, such as electrostatic attraction, chemical interactions, and intra-diffusion (Dinh et al., 2020b).

The mass transfer of Ni(II) ions is accurately described via the relationship graph between Q_e and the square root of time $t^{1/2}$, as presented in Fig. 4b. Accordingly, the process of eliminating Ni(II) from aqueous solution by RM/CS consists of three stages: (i) First, Ni(II) ions relocate quickly to the surface of the adsorbent (also called external diffusion); (ii) next, Ni(II) ions migrate from the surface of the adsorbent to the pores of RM/CS (intra-diffusion process); (iii) finally, the interaction occurs between Ni(II) ions and adsorption sites on the surface of the material by physical or chemical interactions when the adsorption obtains the equilibrium.

During stage 1, Ni(II) ions, positively charged, interact with the material's surface via electrostatic interaction due to their opposite charges. Clearly, at the investigated pH value, functional groups of CS of RM/CS, such as $-\text{OH}$, $-\text{COOH}$ (Matusiak et al., 2022, Wang & Zhuang, 2022), are deprotonated, leading to the surface of RM/CS being charged negatively, as shown in Eqs. (3) and (4). As a result, electrostatic attraction is formed between Ni(II) and RM/CS, as shown in Eqs. (5) and (6).



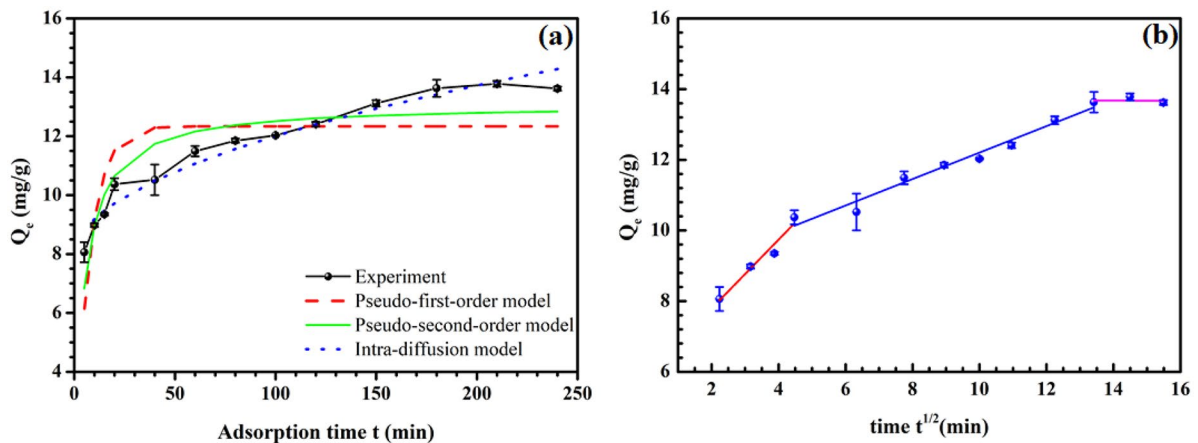


Fig. 4 Plots of kinetic models of the Ni(II) adsorption of RM/CS (a) and Q_e vs $t^{1/2}$ (b) (initial concentration = 50 mg.L⁻¹, pH = 6, adsorbent mass = 0.1 g, shaking speed = 150 rpm)

During stage 2, Ni(II) ions can be diffused into the pores of RM/CS. From the obtained SEM image of RM/CS, it is clear that this material includes many defects, monovacancies, or vacancy clusters, which are suitable for the Ni(II) uptake. This is consistent with the C value calculated from the intra-diffusion model.

At the equilibrium stage, Ni(II) ions continuously interact with the surface of RM/CS via electrostatic attraction and/or the formation of the complex. Notwithstanding, the calculated enthalpy standard (ΔH^0) to be smaller than 40 kJ.mol⁻¹ showed that physical adsorption, namely electrostatic interaction, plays a primary role in the Ni(II) removal of RM/CS.

Adsorption isotherms

Figure 5a–c denote the curves of the Langmuir, Freundlich, and Sips isotherm models of the Ni(II) adsorption of RM/CS at 298 K, 313 K, and 323 K. The corresponding calculated parameters are listed in Supplementary Table S2. As shown in the results, the Sips model is the best fitting model for the experimental data because of its largest correlation coefficient R^2 as well as the smallest RMSE and χ^2 values among the three examined models. Notably, the α_s calculated from the Sips model at 298 K is zero, which confirms this reduces to the Freundlich model related to the multi-layer adsorption of Ni(II). However, these α_s values at higher temperatures (313 K and 323 K) differing from zero indicate that the Ni(II) uptake of RM/CS from aqueous solution is mainly based on both monolayer and

multi-layer adsorption depended on the Ni(II) initial concentration. This can be explained by the Van der Waals force between Ni(II) ions being decreased when increasing the temperature, resulting in a change from multi-layer adsorption (Freundlich model) to monolayer adsorption (Langmuir model). These findings are absolutely consistent with the evaluated nonlinear parameters at 313 K and 323 K. For example, comparing the R^2 , RMSE, and χ^2 values shows that the Freundlich model gives the best fit with experimental data at 298 K and 313 K, but these data fit Langmuir more than the former at 323 K. Furthermore, the determined Langmuir constant K_L is 0.4992 at 323 K ($0 < K_L < 1$), indicating that the Ni(II) uptake of this material is favorable (Al-Ghouthi & Da'ana, 2020). The maximum adsorption capacity of RM/CS for Ni(II) calculated from the Langmuir model is 31.66 mg.g⁻¹ at 323 K, higher than RM and some other natural materials (Table 1).

Thermodynamic studies

The combination of thermodynamic parameters (enthalpy standard (ΔH^0), entropy standard (ΔS^0), and Gibbs free-energy standard (ΔG^0)) and isotherm and kinetic parameters give a complete insight into the behavior of reactions as well as propose technique measures for the treatment of contaminants via the adsorption process (Al-Ghouthi & Al-Absi, 2020). The relation of these thermodynamic parameters is determined via the Van't Hoff equation as given (Dinh et al., 2020b; Mondal et al., 2017):

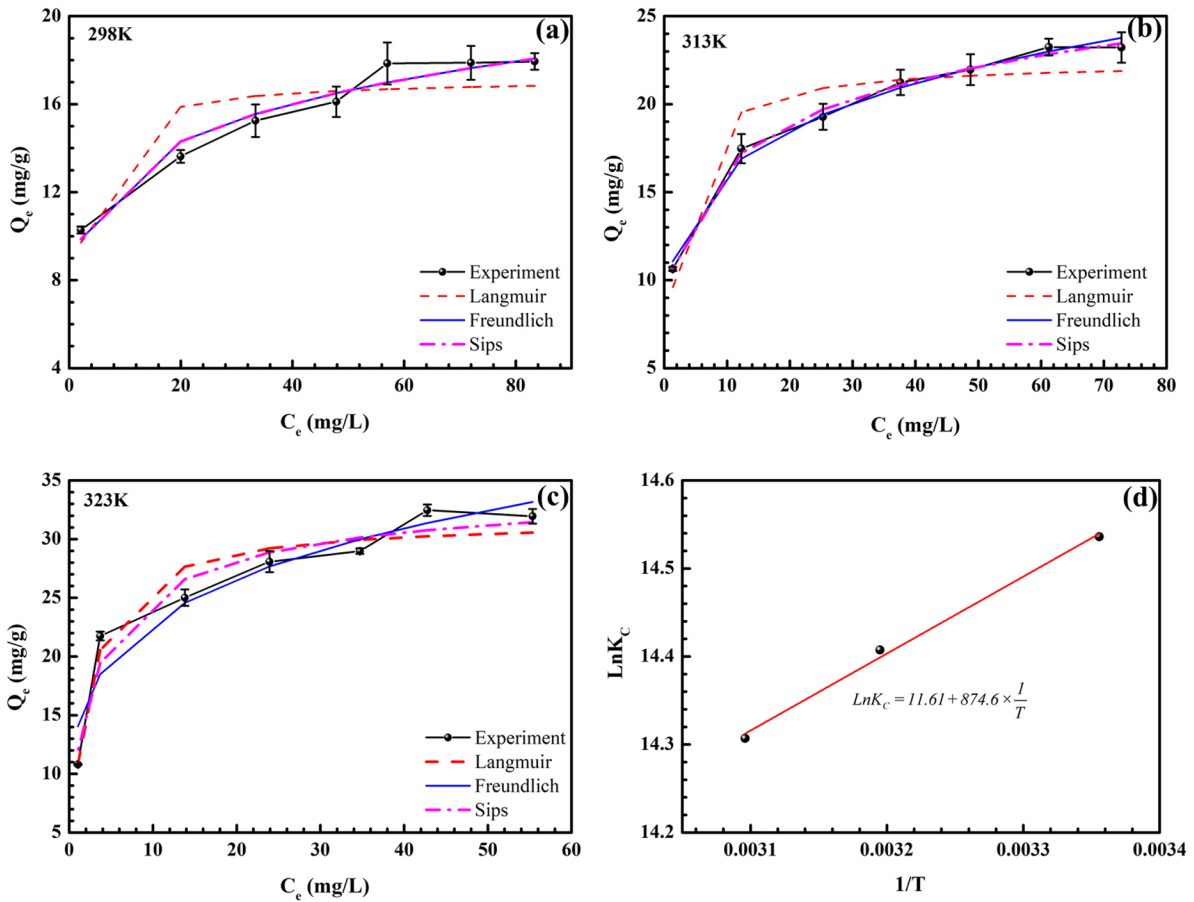


Fig. 5 Plots of isotherm models of the Ni(II) adsorption of RM/CS at 298 K (a), 313 K (b), and 323 K (c); $\ln K_C$ vs. $1/T$ (d) (initial concentration = 20 – 120 $\text{mg}\cdot\text{L}^{-1}$, pH = 6, time = 180 min, adsorbent mass = 0.1 g, shaking speed = 150 rpm)

$$\Delta G^0 = \Delta H^0 - T\Delta S^0, \tag{7}$$

where ΔG^0 can be determined as the following equation:

$$\Delta G^0 = -RT\ln K_C, \tag{8}$$

where the equilibrium constant of K_C is related to the Langmuir constant (K_L) via the following equation (Dinh et al., 2020a; Zhou & Zhou, 2014):

$$K_C = K_L \times M \times 55.5 \times 10^3, \tag{9}$$

where M is the molecular weight of the adsorbate.

By combining Eqs. (7) and (8), the related equation of K_C , ΔH^0 , and ΔS^0 is depicted as

$$\ln K_C = \frac{\Delta S^0}{R} - \frac{\Delta H^0}{RT}. \tag{10}$$

Figure 5d presents the plot of $\ln K_C$ versus $1/T$, and Table 2 lists thermodynamic parameters calculated based on the slope as well as the interception of the graph. Results show that the Ni(II) removal of RM/CS is favorable and spontaneous because the obtained ΔG^0 values are negative at all investigated temperatures. This finding corresponds with the values of n calculated from the Freundlich model. Furthermore, the positive entropy standard ($\Delta S^0 = 96.49 \text{ J}\cdot\text{mol}^{-1}$) shows that during Ni(II) adsorption, the disorderliness in the solid-solution system increases due to a decrease in intermolecular forces temperature rises. This also reconfirms the correlation between isotherm models and examined temperatures in the section on adsorption isotherms. Besides, the negative enthalpy change ($\Delta H^0 = -7.27 \text{ kJ}\cdot\text{mol}^{-1}$) proposes that the Ni(II) uptake is an exothermic process and follows

Table 1 The maximum adsorption capacities of some natural materials

Biosorbents	Optimal adsorption conditions	Q_m (mg.g ⁻¹)	Ref
Peat	pH=5, t=60 min, 298 K	61.27	Bartczak et al. (2018)
Barley straw	pH=4.85, t=24 h, 296 K	35.80	Thevannan et al. (2010)
Cashew nutshell	pH=5, t=30 min, 303 K	18.87	Kumar et al. (2011)
Tea factory waste	pH=4, 298 K	18.42	Malkoc and Nuhoglu (2005)
Na – bentonite	pH=9, 298 K	13.97	Liu and Zhou (2010)
Modified orange peel	pH=5.5, t=150 min, 303 K	9.82	Feng et al. (2011)
Coir pith	pH=7.7, t=10 min, 303 K	9.50	Ewecharoen et al. (2008)
Rice husk	pH=6, t=150 min, 305 K	5.52	Krishnani et al. (2008)
Groundnut shells	pH=5, t=120 min, 308 K	3.80	Shukla and Pai (2005)
Green tea waste	pH=7, t=180 min, 306 K	0.31	Yang et al. (2016)
Red mud	pH=5, t=240 min, 303 K	13.69	Hannachi et al. (2009)
Raw red mud from aluminum industry	pH 5, t=24 h, 294 K	27.40	Smičiklas et al. (2013)
Red mud	pH=5, t=24 h, 293 K	21.72	Smiljanić et al. (2010)
Chitosan	pH=6, t=120 min	10.00	Hydari et al. (2012)
Chitosan beads	pH 5.92, t=24 h, 303 K	45.48	Liao et al. (2016)
RM/CS	pH=6, t=180 min, 323 K	31.66	This study

Table 2 Thermodynamic parameters

T (K)	K_L	K_C	ΔH (kJ.mol ⁻¹)	ΔS (J.mol ⁻¹)	ΔG (kJ.mol ⁻¹)
298	0.6278	2.06×10^6	-7.27	96.49	-36.02
313	0.5520	1.81×10^6			-37.47
323	0.49920	1.63×10^6			-38.44

physical adsorption because the absolute value of enthalpy is smaller than 40 kJ/mol (Bayramoglu et al., 2009).

Conclusion

The obtained results clearly show that the modification of RM successfully synthesized the novel RM/CS material by chitosan. This material was used as the adsorbent to remove Ni(II) from the aqueous solution efficiently. The Ni(II) uptake followed the Sips model and was controlled by the intra-diffusion kinetic model. Adsorption is an exothermic and physical process. The maximum adsorption uptake calculated from the Langmuir model was 31.66 mg.g⁻¹ at 323 K, higher than several other biosorbents, such as red mud, chitosan, and cashew nutshell. This material performs excellent properties that can be used as a potential adsorbent to remove Ni(II) from wastewater.

Data availability Not applicable.

Declarations

Competing interests The authors declare no competing interests.

References

Aigbe, U. O., et al. (2021). Fly ash-based adsorbent for adsorption of heavy metals and dyes from aqueous solution: A review. *Journal of Materials Research and Technology*, 14, 2751–2774.

Al-Ghouti, M. A., & Al-Absi, R. S. (2020). Mechanistic understanding of the adsorption and thermodynamic aspects of cationic methylene blue dye onto cellulosic olive stones biomass from wastewater. *Scientific Reports*, 10, 15928.

Al-Ghouti, M. A., & Da'ana, D. A. (2020). Guidelines for the use and interpretation of adsorption isotherm models: A review. *Journal of Hazardous Materials*, 393, 122383.

Bartczak, P., et al. (2018). Removal of nickel (II) and lead (II) ions from aqueous solution using peat as a low-cost adsorbent: A

- kinetic and equilibrium study. *Arabian Journal of Chemistry*, 11, 1209–1222.
- Bayramoglu, G., Altintas, B., & Arica, M. Y. (2009). Adsorption kinetics and thermodynamic parameters of cationic dyes from aqueous solutions by using a new strong cation-exchange resin. *Chemical Engineering Journal*, 152, 339–346.
- Çelebi, H., Gök, G., & Gök, O. (2020). Adsorption capability of brewed tea waste in waters containing toxic lead (II), cadmium (II), nickel (II), and zinc (II) heavy metal ions. *Scientific Reports*, 10, 17570.
- de Jesus, C. P. C., et al. (2015). Removal of reactive dye from aqueous solution using thermally treated red mud. *Desalination and Water Treatment*, 55, 1040–1047.
- Deng, X., Qi, L., & Zhang, Y. (2018). Experimental study on adsorption of hexavalent chromium with microwave-assisted alkali modified fly ash. *Water, Air, & Soil Pollution*, 229, 18.
- Dinh, V.-P., et al. (2020a). Chitosan-MnO₂ nanocomposite for effective removal of Cr (VI) from aqueous solution. *Chemosphere*, 257, 127147.
- Dinh, V.-P., et al. (2020b). Primary biosorption mechanism of lead (II) and cadmium (II) cations from aqueous solution by pomelo (*Citrus maxima*) fruit peels. *Environmental Science and Pollution Research*, 28, 63504–63515.
- Ewecharoen, A., Thiravetyan, P., & Nakbanpote, W. (2008). Comparison of nickel adsorption from electroplating rinse water by coir pith and modified coir pith. *Chemical Engineering Journal*, 137, 181–188.
- Feng, N., et al. (2011). Biosorption of heavy metals from aqueous solutions by chemically modified orange peel. *Journal of Hazardous Materials*, 185, 49–54.
- Hamza, M. F., et al. (2019). Synthesis and adsorption characteristics of grafted hydrazinyl amine magnetite-chitosan for Ni(II) and Pb(II) recovery. *Chemical Engineering Journal*, 362, 310–324.
- Hannachi, Y., Shapovalov, N. A., & Hannachi, A. (2009). Adsorption of nickel from aqueous solution by the use of low-cost adsorbents. *Desalination and Water Treatment*, 12, 276–283.
- Hydari, S., et al. (2012). A comparative investigation on removal performances of commercial activated carbon, chitosan biosorbent and chitosan/activated carbon composite for cadmium. *Chemical Engineering Journal*, 193–194, 276–282.
- Khairul, M. A., Zanganeh, J., & Moghtaderi, B. (2019). The composition, recycling and utilisation of Bayer red mud. *Resources, Conservation and Recycling*, 141, 483–498.
- Khajavian, M., et al. (2019). Simultaneous biosorption of nickel and cadmium by the brown algae *Cystoseria indica* characterized by isotherm and kinetic models. *Applied Biological Chemistry*, 62, 69.
- Krishnani, K. K., et al. (2008). Biosorption mechanism of nine different heavy metals onto biomatrix from rice husk. *Journal of Hazardous Materials*, 153, 1222–1234.
- Kumar, P. S., et al. (2011). Adsorption behavior of nickel (II) onto cashew nut shell: Equilibrium, thermodynamics, kinetics, mechanism and process design. *Chemical Engineering Journal*, 167, 122–131.
- Li, P., et al. (2019). Recover iron from bauxite residue (Red Mud). *IOP Conference Series: Earth and Environmental Science*, 252, 042037.
- Liao, B., et al. (2016). Equilibriums and kinetics studies for adsorption of Ni(II) ion on chitosan and its triethylenetetramine derivative. *Colloids and Surfaces a: Physicochemical and Engineering Aspects*, 501, 32–41.
- Liu, Z.-r., & Zhou, S.-q. (2010). Adsorption of copper and nickel on Na-bentonite. *Process Safety and Environmental Protection*, 88, 62–66.
- Luu, T.-T., et al. (2022). Pb(II) adsorption mechanism and capability from aqueous solution using red mud modified by chitosan. *Chemosphere*, 287, 132279.
- Lyklema, J. (1984). Points of zero charge in the presence of specific adsorption. *Journal of Colloid and Interface Science*, 99, 109–117.
- Lyu, F., et al. (2021). Efficient removal of Pb(II) ions from aqueous solution by modified red mud. *Journal of Hazardous Materials*, 406, 124678.
- Malkoc, E., & Nuhoglu, Y. (2005). Investigations of nickel (II) removal from aqueous solutions using tea factory waste. *Journal of Hazardous Materials*, 127, 120–128.
- Matusiak, J., et al. (2022). The journey of tuning chitosan properties in colloidal systems: Interactions with surfactants in the bulk and on the alumina surface. *Chemical Engineering Journal*, 450, 138145.
- Mondal, N. K., et al. (2017). Optimization of Cr (VI) biosorption onto *Aspergillus niger* using 3-level Box-Behnken design: Equilibrium, kinetic, thermodynamic and regeneration studies. *Journal of Genetic Engineering and Biotechnology*, 15, 151–160.
- Ni, F., et al. (2015). Preparation and characterization of a cost-effective red mud/polyaluminum chloride composite coagulant for enhanced phosphate removal from aqueous solutions. *Journal of Water Process Engineering*, 6, 158–165.
- Pap, S., et al. (2020). Synthesis optimisation and characterisation of chitosan-calcite adsorbent from fishery-food waste for phosphorus removal. *Environmental Science and Pollution Research*, 27, 9790–9802.
- Sahu, M. K., et al. (2013). Removal of Pb(II) from aqueous solution by acid activated red mud. *Journal of Environmental Chemical Engineering*, 1, 1315–1324.
- Shukla, S. R., & Pai, R. S. (2005). Adsorption of Cu(II), Ni(II) and Zn(II) on dye loaded groundnut shells and sawdust. *Separation and Purification Technology*, 43, 1–8.
- Smičiklas, I., et al. (2013). The influence of citrate anion on Ni(II) removal by raw red mud from aluminum industry. *Chemical Engineering Journal*, 214, 327–335.
- Smičiklas, I., et al. (2014). Effect of acid treatment on red mud properties with implications on Ni(II) sorption and stability. *Chemical Engineering Journal*, 242, 27–35.
- Smiljanić, S., et al. (2010). Rinsed and thermally treated red mud sorbents for aqueous Ni²⁺ ions. *Chemical Engineering Journal*, 162, 75–83.
- Supanchaiyamat, N., et al. (2019). Lignin materials for adsorption: Current trend, perspectives and opportunities. *Bioresource Technology*, 272, 570–581.
- Taneez, M., & Hurel, C. (2019). A review on the potential uses of red mud as amendment for pollution control in environmental media. *Environmental Science and Pollution Research*, 26, 22106–22125.
- Thevannan, A., Mungroo, R., & Niu, C. H. (2010). Biosorption of nickel with barley straw. *Bioresource Technology*, 101, 1776–1780.

- Vakili, M., et al. (2019). Regeneration of chitosan-based adsorbents used in heavy metal adsorption: A review. *Separation and Purification Technology*, 224, 373–387.
- Wang, M., & Liu, X. (2021). Applications of red mud as an environmental remediation material: A review. *Journal of Hazardous Materials*, 408, 124420.
- Wang, J., & Zhuang, S. (2022). Chitosan-based materials: Preparation, modification and application. *Journal of Cleaner Production*, 355, 131825.
- Wang, L., et al. (2019). Application of red mud in wastewater treatment. *Minerals*, 9, 281.
- Yang, S., et al. (2016). Mono/competitive adsorption of Arsenic(III) and Nickel(II) using modified green tea waste. *Journal of the Taiwan Institute of Chemical Engineers*, 60, 213–221.
- Yang, T., et al. (2020). Enhancing Cd(II) sorption by red mud with heat treatment: Performance and mechanisms of sorption. *Journal of Environmental Management*, 255, 109866.
- Zhang, L., et al. (2016). Crosslinked quaternized chitosan/bentonite composite for the removal of Amino black 10B from aqueous solutions. *International Journal of Biological Macromolecules*, 93, 217–225.
- Zhou, X., & Zhou, X. (2014). The unit problem in the thermodynamic calculation of adsorption using the Langmuir equation. *Chemical Engineering Communications*, 201, 1459–1467.
- Zhu, W., et al. (2017). Investigating the heavy metal adsorption of mesoporous silica materials prepared by microwave synthesis. *Nanoscale Research Letters*, 12, 323.

Publisher's Note Springer Nature remains neutral with regard to jurisdictional claims in published maps and institutional affiliations.

Springer Nature or its licensor (e.g. a society or other partner) holds exclusive rights to this article under a publishing agreement with the author(s) or other rightsholder(s); author self-archiving of the accepted manuscript version of this article is solely governed by the terms of such publishing agreement and applicable law.